Supplement of

Estimating seasonal bulk density of level sea ice using the data derived from in situ and ICESat-2 synergistic observations during MOSAiC

Yi Zhou et al.

Correspondence: Xianwei Wang (xianwei.wang@sjtu.edu.cn) and Ruibo Lei (leiruibo@pric.org.cn)

Table S1. Overview of the 12 SIMBAs and 3 SIMBs deployed within the MOSAiC DN.

Buoy name	Start date (YYYY/MM/DD)	End date (YYYY/MM/DD)	Onset of growth (YYYY/MM/DD)	Initial ice thickness (m)	Initial snow depth (m)	Growth rate* (m per month)	Ice type
SIMBA _T47	2019/10/13	2020/02/07	2020/10/16	0.34	0.10	0.23	FYI
SIMBA _T58	2019/10/07	2020/07/21	2019/11/09	0.84	0.08	0.16	SYI
SIMBA _T62	2019/10/29	2020/07/27	2019/11/02	0.80	0.20	0.16	SYI
SIMBA _T63	2019/10/07	2020/07/28	2019/11/28	1.12	0.14	0.12	SYI
SIMBA _T64	2019/10/10	2020/08/02	2019/11/22	1.74	0.16	0.10	SYI
SIMBA _T65	2019/10/07	2020/05/30	2019/12/08	1.32	0.14	0.10	SYI
SIMBA _T66	2019/10/29	2020/08/03	2019/10/30	0.40	0.10	0.19	FYI
SIMBA _T67	2019/11/09	2020/08/03	2019/11/14	1.36	0.22	0.12	SYI
SIMBA _T68	2019/10/05	2020/06/05	2019/12/05	1.81	0.17	0.08	SYI
SIMBA _T69	2019/10/11	2020/01/31	2019/10/29	0.80	0.08	0.13	SYI
SIMBA _T70	2019/10/09	2020/08/05	2019/10/14	0.48	0.06	0.21	FYI
SIMBA _T72	2019/10/09	2020/04/27	2019/11/02	1.00	0.14	0.18	SYI
SIMB_I1	2019/10/05	2020/03/15	2019/12/17	1.20	0.17	0.11	SYI
SIMB_I2	2019/10/07	2020/07/30	2019/11/10	0.80	0.12	0.17	SYI
SIMB_I3	2019/10/10	2019/02/03	2019/10/10	0.30	0.06	0.31	FYI

*Growth rates of sea ice thickness for different buoys from mid-October to mid-April. Note that the statistical test *P*-values are all below 0.001.

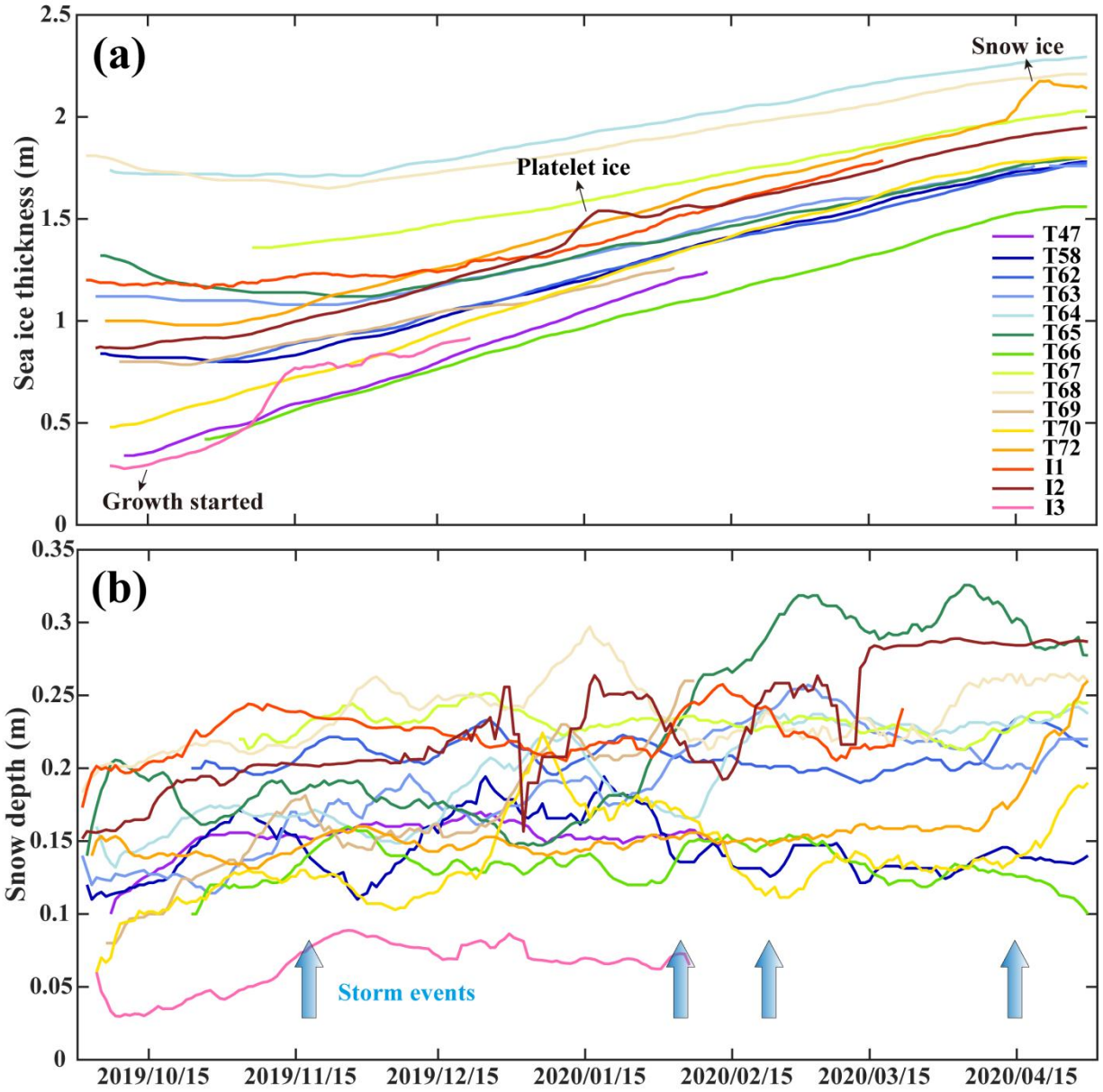

Figure S1. Variations in **(a)** sea ice thickness and **(b)** snow depth for each buoy site during the MOSAiC freezing season. **Note:** The peculiarities of sites T72, I2 and I3 (as described in the text) are indicated by black arrows in panel **(a)**, and the storm events are indicated by blue arrows in panel **(b)** according to Wagner et al. (2022).

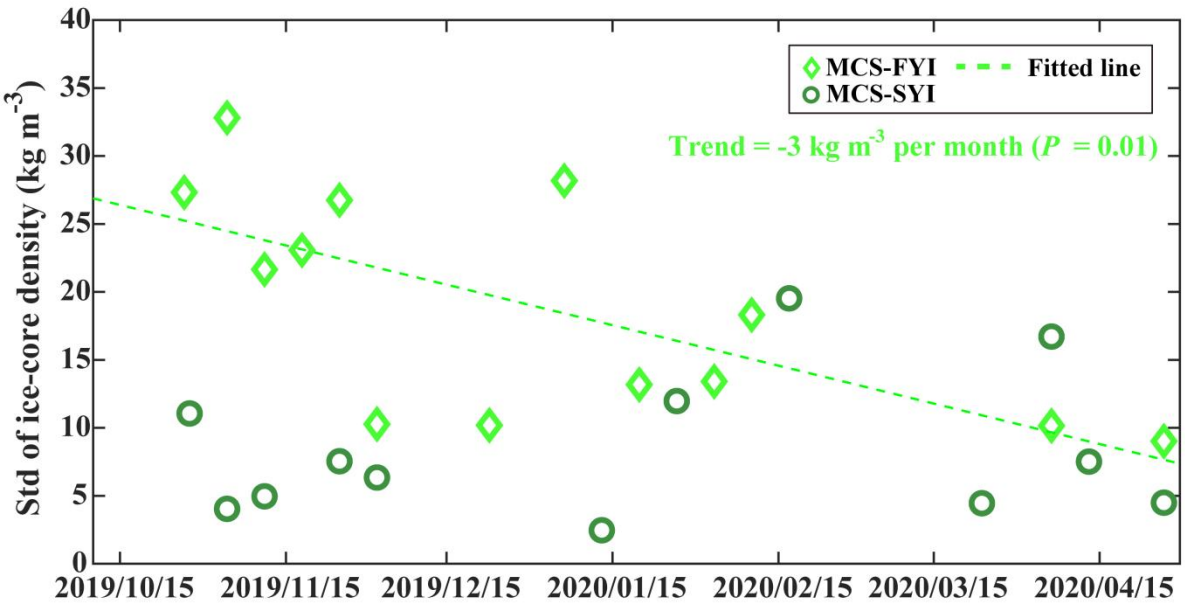

Figure S2. Standard deviation (Std) of core-based IBD estimates during the study period, and the dashed line shows the linear trend of MCS-FYI (P = 0.01).

Text S1. Feasibility of the modal approach

Two principal arguments support the feasibility of the modal method: First, at regional scales (approximately tens of kilometers), Arctic sea ice freeboard and thickness follow a log-normal or exponential distribution (Haas, 2010; Farrell et al., 2011; Petty et al., 2016; Landy et al., 2019). Second, the mode of the ice freeboard or thickness distribution obtained from satellite measurements accurately represents ice growth driven by thermodynamic forcing (Ricker et al., 2015; Koo et al., 2021). In essence, the mode of the freeboard (or thickness) distribution acts as a reliable indicator of level ice, excluding the impacts of deformed ice components. This property proves advantageous for estimating the IBD of level ice using the hydrostatic equilibrium method (Hutchings et al., 2015).

However, it is important to emphasize that total freeboard includes information on snow accumulation, potentially influencing the distribution characteristics of the sea ice itself. In this context, we investigated whether the mode of the total freeboard distribution still represents the average total freeboard of the level ice components, using total freeboard data from AWI IceBird airborne measurements (Fig. S3). Overall, the two freeboard values closely align, with their relative percentage differences (RPD) exceeding 90 % in daily records containing at least 20 % level ice, thereby demonstrating the effectiveness of the modal method.

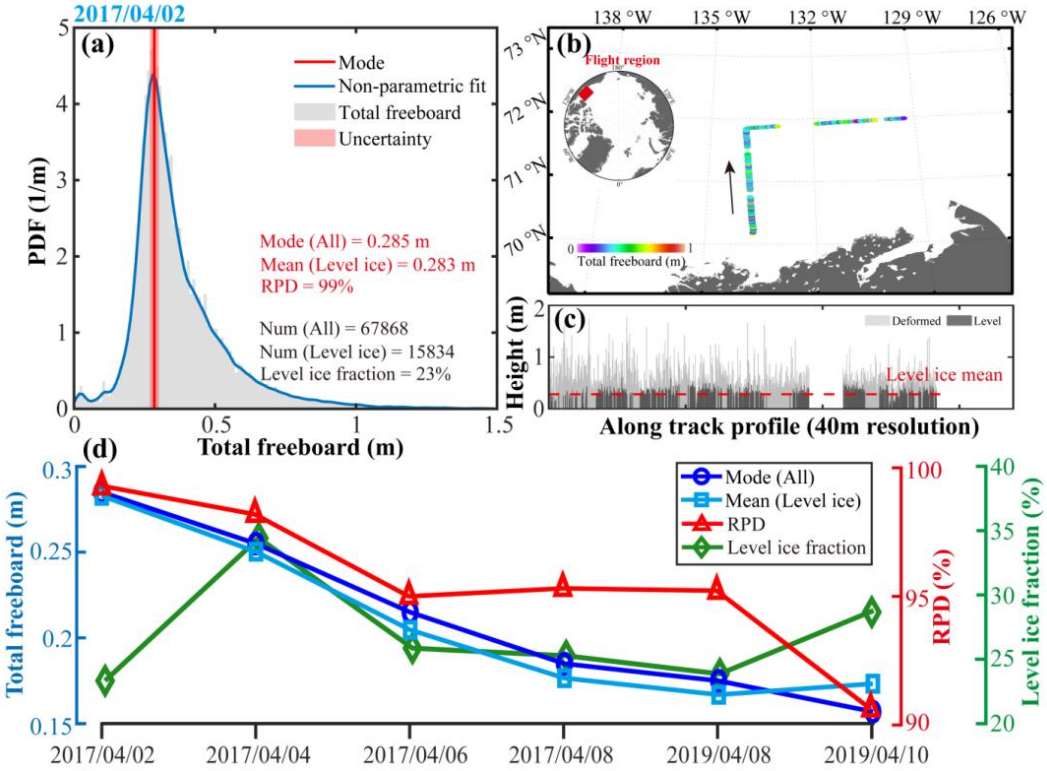

Figure S3. Comparison of the mode of the total freeboard distribution (encompassing all surface types) with the mean total freeboard of level ice, derived from AWI IceBird measurements conducted in April 2017 and April 2019. The example from 2 April 2017 illustrates: **(a)** the total freeboard distribution, **(b)** the measurement area, and **(c)** the total freeboard profile. **(d)** Results for each measurement date include the modal freeboard for all surface types, mean freeboard for level ice, and the relative percentage difference (RPD) between the two freeboard values, as well as the level ice fraction (at least 20%).

Text S2. Spatial scale adjustments for airborne and satellite measurements

It is essential to recognize that the spatial scale of airborne and satellite measurements significantly exceeds that of the IMB array, posing potential challenges for spatial compatibility in calculating IBD using the hydrostatic equilibrium method. Nevertheless, the buoy array is anticipated to capture a broader range of sea ice and snow variations than those observed at its deployment sites (Koo et al., 2021; von Albedyll et al., 2022), also shown in Fig. 4. Here, an indirect method was utilized to examine potential spatial scale differences and to facilitate preliminary adjustments. Specifically, the mean snow depths of the IMBs were deducted from the modal total freeboards from airborne and satellite measurements at the DN and L-site scales, respectively. The results unexpectedly revealed that the differences (i.e., sea ice freeboard) were negative during the early freezing season, showing a trend of initially decreasing negative values, which then transitioned to increasing positive values (Fig. S4). However, based on early in situ observations from buoy deployments and ice cores, the significantly negative sea ice freeboard observed is deemed unrealistic, thereby suggesting significant spatial incompatibility issues.

Given the expected similar variations between the buoy array and the broader range averages, the modal total freeboards were systematically adjusted at both the DN and L-site scales to be compatible with the buoy array sites. Specifically, the adjustment at the corresponding scale represents the sum of two terms, 1) the absolute value of the maximum negative sea ice freeboard (original modal total freeboard minus buoy snow depth), and 2) the reference sea ice freeboard obtained from the FYI and SYI cores in late October, which was determined by weighting the FYI/SYI fractions from the corresponding buoy array sites. The relatively good agreement between ice core and buoy observations during the early stages supports the use of the initial ice core freeboard as the adjustment reference (see details in Section 3.1). In this way, we ensured that the difference between the adjusted modal total freeboard and the snow depth at the buoy array sites could reasonably represent the sea ice freeboard during MOASiC, thus ensuring compatibility between the buoy array and airborne/satellite measurements used in the hydrostatic equilibrium calculation (Fig. S4).

Overall, the modal total freeboards were systematically adjusted upwards by a fixed value of ~0.07 m at both DN and L-site scales to match the buoy array sites throughout the study period. Due to the lack of mutual evaluation for different MOSAiC observations prior to late October, IBD retrievals excluded the adjusted modal total freeboard records from this period. Here, we suggest that the spatial scale adjustment term is closely related to the redistribution of snow depth across the MOSAiC ice floes (see details in Section 3.1). These spatial adjustments are not expected to impact the seasonality of IBD, but rather its relative magnitude. Furthermore, Section 3.1 highlights

the spatial heterogeneity of the MOSAiC ice floes, Section 3.2 validates the robustness of the spatial scale adjustments, and Section 4.1 offers a detailed analysis of how the reference value settings affect the IBD estimates.

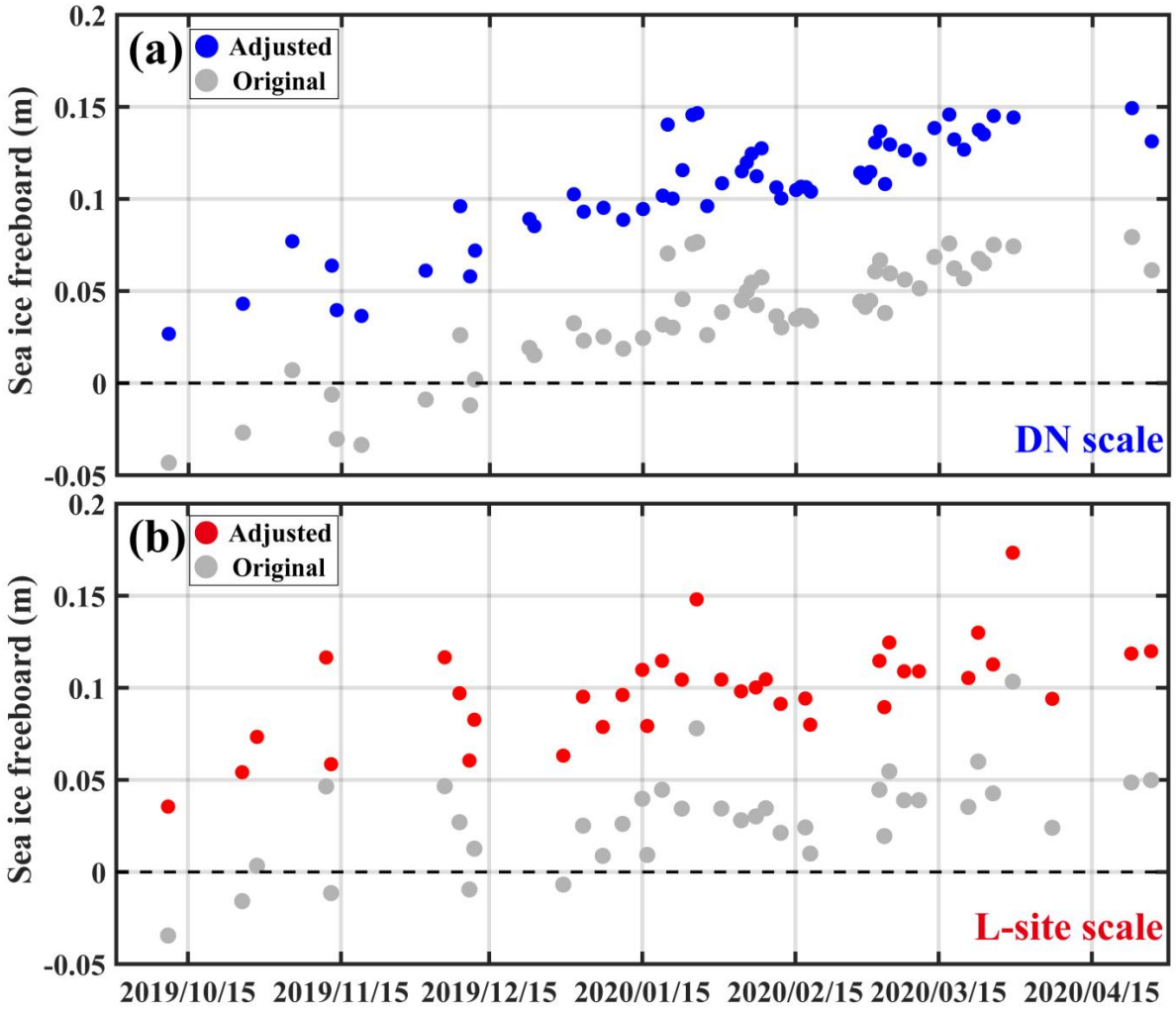

Figure S4. Seasonal variation of sea ice freeboard during the MOSAiC expedition. Sea ice freeboard is calculated by subtracting buoy-derived mean snow depth from both adjusted and original modal total freeboards at the **(a)** DN and **(b)** L-site scales, respectively. Zero sea ice freeboard is indicated by a black dashed line.

Text S3. Relative contribution of the input parameters for IBD retrieval

In order to quantify which input parameters used in Eq. (2) contribute most or least to the total uncertainty in sea ice bulk density, the relative contribution of the input parameters (RC_{X}) was defined as follows:

$$RC_{\mathrm{X}} = \frac{(\frac{\partial \rho_{\mathrm{i}}}{\partial X})^2 \times {\sigma_X}^2}{{\sigma_{\rho_{\mathrm{i}}}}^2} \times 100\% \tag{S1}$$

where $\sigma_{\rho_{\mathrm{i}}}$ is the uncertainty in sea ice bulk density, X and σ_X denote each input parameter and its uncertainty, respectively.

The partial derivatives of sea ice bulk density with respect to each variable are as follows:

$$\frac{\partial \rho_{\mathrm{i}}}{\partial \rho_{\mathrm{w}}} = \left(1 - \frac{h_{\mathrm{f}}}{h_{\mathrm{i}}} + \frac{h_{\mathrm{s}}}{h_{\mathrm{i}}}\right) \tag{S2}$$

$$\frac{\partial \rho_{\mathrm{i}}}{\partial \rho_{\mathrm{s}}} = -\frac{h_{\mathrm{s}}}{h_{\mathrm{i}}} \tag{S3}$$

$$\frac{\partial \rho_{\mathrm{i}}}{\partial h_{\mathrm{i}}} = \frac{\rho_{\mathrm{w}} h_{\mathrm{f}} - \rho_{\mathrm{w}} h_{\mathrm{s}} + \rho_{\mathrm{s}} h_{\mathrm{s}}}{{h_{\mathrm{i}}}^2} \tag{S4}$$

$$\frac{\partial \rho_{\mathrm{i}}}{\partial h_{\mathrm{s}}} = \frac{\rho_{\mathrm{w}} - \rho_{\mathrm{s}}}{h_{\mathrm{i}}} \tag{S5}$$

$$\frac{\partial \rho_{\mathrm{i}}}{\partial h_{\mathrm{f}}} = -\frac{\rho_{\mathrm{w}}}{\mathrm{h_i}} \tag{S6}$$

where ρ_{i} is the sea ice bulk density, ρ_{w} and ρ_{s} represent the seawater and snow bulk densities, respectively; h_{i}, h_{f}, and h_{s} are the sea ice thickness, total freeboard, and snow depth, respectively.

References

Farrell, S. L., Kurtz, N., Connor, L. N., Elder, B. C., Leuschen, C., Markus, T., McAdoo, D. C., Panzer, B., Richter-Menge, J., and Sonntag, J. G.: A first assessment of IceBridge snow and ice thickness data over Arctic sea ice, IEEE Transactions on Geoscience and Remote Sensing, 50, 2098-2111, https://doi.org/10.1109/tgrs.2011.2170843, 2011.

Haas, C.: Dynamics versus thermodynamics: The sea ice thickness distribution, Sea ice, 82, 113-152, https://doi.org/10.1002/9781444317145.ch4, 2010.

Hutchings, J. K., Heil, P., Lecomte, O., Stevens, R., Steer, A., and Lieser, J. L.: Comparing methods of measuring sea-ice density in the East Antarctic, Annals of Glaciology, 56, 77-82, https://doi.org/10.3189/2015aog69a814, 2015.

Koo, Y., Lei, R., Cheng, Y., Cheng, B., Xie, H., Hoppmann, M., Kurtz, N. T., Ackley, S. F., and Mestas-Nuñez, A. M.: Estimation of thermodynamic and dynamic contributions to sea ice growth in the Central Arctic using ICESat-2 and MOSAiC SIMBA buoy data, Remote Sensing of Environment, 267, 112730, https://doi.org/10.1016/j.rse.2021.112730, 2021.

Landy, J. C., Tsamados, M., and Scharien, R. K.: A Facet-Based Numerical Model for Simulating SAR Altimeter Echoes From Heterogeneous Sea Ice Surfaces, IEEE Transactions on Geoscience and Remote Sensing, 57, 4164-4180, https://doi.org/10.1109/tgrs.2018.2889763, 2019.

Petty, A. A., Tsamados, M. C., Kurtz, N. T., Farrell, S. L., Newman, T., Harbeck, J. P., Feltham, D. L., and Richter-Menge, J. A.: Characterizing Arctic sea ice topography using high-resolution IceBridge data, The Cryosphere, 10, 1161-1179, https://doi.org/10.5194/tc-10-1161-2016, 2016.

Ricker, R., Hendricks, S., Perovich, D. K., Helm, V., and Gerdes, R.: Impact of snow accumulation on CryoSat-2 range retrievals over Arctic sea ice: An observational approach with buoy data, Geophysical Research Letters, 42, 4447-4455, https://doi.org/10.1002/2015gl064081, 2015.

von Albedyll, L., Hendricks, S., Grodofzig, R., Krumpen, T., Arndt, S., Belter, H. J., Birnbaum, G., Cheng, B., Hoppmann, M., Hutchings, J., Itkin, P., Lei, R., Nicolaus, M., Ricker, R., Rohde, J., Suhrhoff, M., Timofeeva, A., Watkins, D., Webster, M., and Haas, C.: Thermodynamic and dynamic contributions to seasonal Arctic sea ice thickness distributions from airborne observations, Elementa: Science of the Anthropocene, 10, https://doi.org/10.1525/elementa.2021.00074, 2022.

Wagner, D. N., Shupe, M. D., Cox, C., Persson, O. G., Uttal, T., Frey, M. M., Kirchgaessner, A., Schneebeli, M., Jaggi, M., Macfarlane, A. R., Itkin, P., Arndt, S., Hendricks, S., Krampe, D., Nicolaus, M., Ricker, R., Regnery, J., Kolabutin, N., Shimanshuck, E., Oggier, M., Raphael, I., Stroeve, J., and Lehning, M.: Snowfall and snow accumulation during the MOSAiC winter and spring seasons, The Cryosphere, 16, 2373-2402, https://doi.org/10.5194/tc-16-2373-2022, 2022.